DOI: 10.1021/cg1002379

CRYSTAL GROWTH & DESIGN Article

2010, Vol. 10
3892–3900

Published as part of a virtual special issue of selected papers presented in celebration of the 40th Anniversary Conference of the British Association for Crystal Growth (BACG), which was held at Wills Hall, Bristol, UK, September 6−8, 2009.

Investigation of the Effect of Temperature Cycling on Surface Features of Sulfathiazole Crystals during Seeded Batch Cooling Crystallization

Mohd R. Abu Bakar,[†,‡] Zoltan K. Nagy,*[,†] and Chris D. Rielly[†]

[†]*Department of Chemical Engineering, Loughborough University, Loughborough, Leicestershire LE11 3TU, United Kingdom, and* [‡]*Kulliyyah of Engineering, International Islamic University Malaysia, Gombak, Selangor Darul Ehsan, Malaysia*

Received February 20, 2010; Revised Manuscript Received June 26, 2010

ABSTRACT: The effect of temperature cycling on the surface features of sulfathiazole crystals was investigated using focused beam reflectance measurement (FBRM) and *ex situ* optical microscopy, scanning electron microscopy (SEM), and atomic forced microscopy (AFM). Smoothing of the crystal surface was observed during heating, while during cooling the smooth crystals showed features growing on their surfaces. These changes on the crystal surface were detected by the FBRM as an increase in the number of coarse counts during heating phases and a drop during cooling phases. Laser beam spreading caused by the surface changes and signal/chord splitting due to the formation of sharp edges are suggested as explanations for the FBRM results. The study shows the capability of FBRM to provide useful information with regard to the changes on the surface of the crystalline products, which could be linked to possible growth mechanisms. The information can be used to avoid problems in the downstream processing or in the final product property due to variations in flowability and friability, which are related to the crystal surface property.

1. Introduction

Temperature cycling, which is an alternating cycle of heating and cooling phases, has been applied in crystallization processes in order to control crystal size distribution,[1−4] to optimize the size of the seed bed for subsequent cooling,[5] and to accelerate crystal growth.[6] The approach also indirectly controls the crystal surface properties, since the heating phases are expected to promote dissolution of the unwanted crystal surface features, such as dendritic features.[5] Smoother crystals may have better flowability and friability than rougher crystals; hence, controlling the surface properties of the crystalline product may have a significant effect on the efficiency of the downstream processes and the quality of the final product. Such a control may be assisted by process analytical technology (PAT) tools that can provide in-process information to indicate surface events and changes in surface features.

Lasentec focused beam reflectance measurement (FBRM) is one of the PAT tools that has been used extensively in crystallization processes for the monitoring of the solid phase. It uses a laser beam sent through fiber optics to an immersion probe tip where it is finely focused by a rotating lens, which causes the beam to scan in a circular path through a sapphire window at a fixed high speed. The beam then passes into the solution under study. When it hits a crystal suspended in the solution, light is scattered in many directions, but only light scattered back toward the probe is collected. The crystal continues to backscatter the light until the beam reaches the opposite edge of the crystal. The time period of the backscattering (Δt) is recorded and multiplied by the scan speed of the beam (v_b) to give a chord length, which is the distance between one edge of the crystal and the other (s). Figure 1 shows a schematic diagram of backscattered light pulses detection and chord length measurement. FBRM allows the monitoring of the change in chord length distribution (CLD) for different chord size classes (fine, intermediate, and coarse) of the crystals as a function of time. It has been successfully used to detect the metastable zone limit, since a sudden increase in the fine chord counts indicates the onset of nucleation.[7−10] Studies have shown that although FBRM performed comparably to the bulk video imaging,[11,12] it detected nucleation the earliest compared to visual observation and attenuated total reflectance Fourier transform infrared spectroscopy.[13] The solubility curve can also be constructed using FBRM, since a reduction in the coarse chord counts corresponds to the dissolution of crystals.[8,10] Since CLD data measured by FBRM provides an approximate correlation to the crystal size distribution (CSD) in slurry, many research groups used FBRM to monitor and control the CSD online.[5,14−19] FBRM has also been utilized to monitor polymorphic transformation[20−23] and to control polymorphic purity.[2,24] However, based on the authors' knowledge, its practical capability in detecting changes in the surface features of crystals with the link to potential growth mechanisms has never been evaluated, although the effect of surface roughness has been taken into

*Corresponding author. Telephone: + 44 (0)1509 222 516. Fax: + 44 (0)1509 223 953. E-mail: Z.K.Nagy@lboro.ac.uk.

 Published on Web 07/27/2010

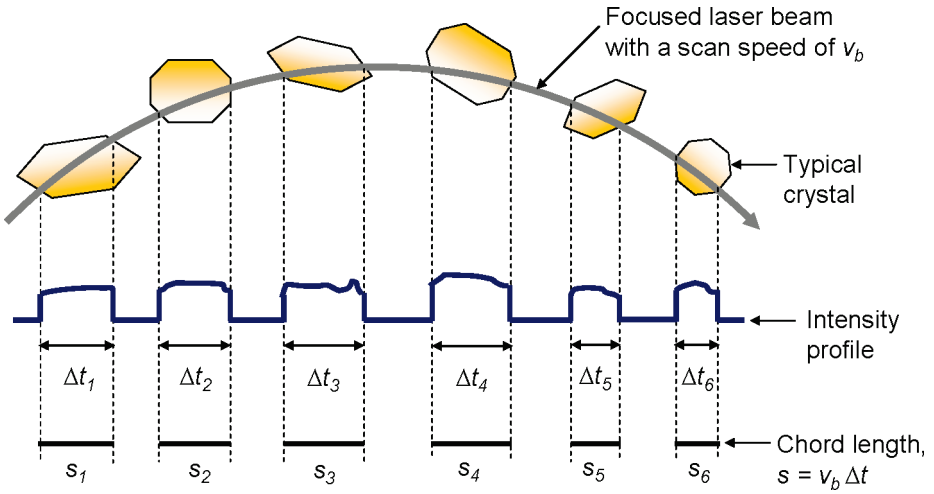

Figure 1. Schematic diagram of backscattered light pulse detection and chord length measurement of typical crystals.

consideration in a method that combined FBRM data and inverse modeling for determining CSD from CLD.[25]

The analytical technique most commonly used to study the surface properties of crystals is microscopy. The technique includes optical microscopy, scanning electron microscopy (SEM), and atomic force microscopy (AFM). Although optical microscopy is considered low-tech compared to the others, it is still a very useful tool, particularly for a rapid preliminary examination in deciding which other studies or techniques are required. Both SEM and AFM can resolve surface features down to nanometer scale, but different types of information about the surface features are given, since their image formation mechanisms are different. For the SEM, the impingement of an electron beam on the surface of a sample results in the emission of a secondary electron, which is detected and its intensity at each data point during the scanning of the electron beam across the surface is used to form a two-dimensional morphological image.[26] For the AFM, the detection of surface forces during scanning a sharp tip (probe) on the end of a flexible cantilever across a sample surface, while maintaining a small, constant force is used to form a three-dimensional or topographical surface image.[27,28] Since the SEM images cannot provide the actual positioning of surface features relative to the mean surface level (i.e., height or depth), they may lead to misinterpretation of the data.[26] For this reason, SEM analysis is normally complemented with AFM analysis, since the latter can provide measurements in three dimensions, including height or depth information.

In this paper, an investigation of the effect of temperature cycling, implemented during seeded batch cooling crystallization of sulfathiazole in water, on the surface features of the crystals is presented. The investigation involves the evaluation of the capability of FBRM as a PAT tool in monitoring surface events and detecting changes in surface features of crystals. The FBRM results were verified by examining the surface appearance of the crystals at the ends of each heating and cooling phase using *ex situ* optical microscopy, SEM, and AFM.

2. Experimental Section

2.1. Materials. Sulfathiazole with a purity of 99% was purchased from Alfa Aesar. The unsieved raw material was also used as seeds. The solvent ultrapure water was generated from a Milli-Q reversed osmosis unit.

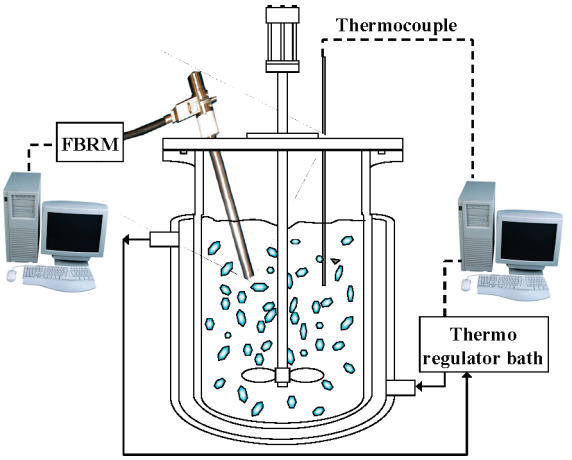

Figure 2. Schematic representation of the experimental setup.

2.2. Apparatus. The crystallization experiments were performed in a jacketed 500 mL glass vessel. The temperature in the vessel was controlled with a PTFE thermocouple connected to a thermo fluid circulator bath (Huber Variostat CC-415 vpc). The temperature readings were recorded every 20 s on a computer by a control interface (Crystallization Process Informatics System—CryPRINS) written in LabVIEW (National Instruments). An overhead stirrer with a PTFE four pitch-bladed turbine was used to agitate the system at 320 rpm. An FBRM probe (model D600, Lasentec) was inserted into the solution to measure chord length distributions. The distributions were collected every 20 s and averaged out during collection. They were monitored using the FBRM control interface software (version 6.7). A schematic representation of the experimental setup is shown in Figure 2.

2.3. Seeded Batch Cooling Crystallization with Temperature Cycling. The initial solution was prepared to have a concentration corresponding to a saturation temperature at 80 °C (i.e., 1.0 g of sulfathiazole per 100 g of water). After it was heated to complete dissolution, the resulting clear solution was cooled to 78 °C and equilibrated at this temperature prior to the loading of seeds. The amount of seeds used was about 10% of the amount of solute in the solution. After the seeds were loaded, the systems were subjected to temperature cycling with temperature fluctuations between 6 and 8 °C at heating/cooling rates of 0.5 °C/min, progressively stepping down toward 20 °C. A repeat of the experiment was performed for sample withdrawal at the end of each heating and cooling phase for microscopy analyses. The samples were vacuum filtered and dried.

2.4. Microscopy Analyses. The sampled crystals were examined for their appearance and surface features using optical microscopy, SEM, and AFM.

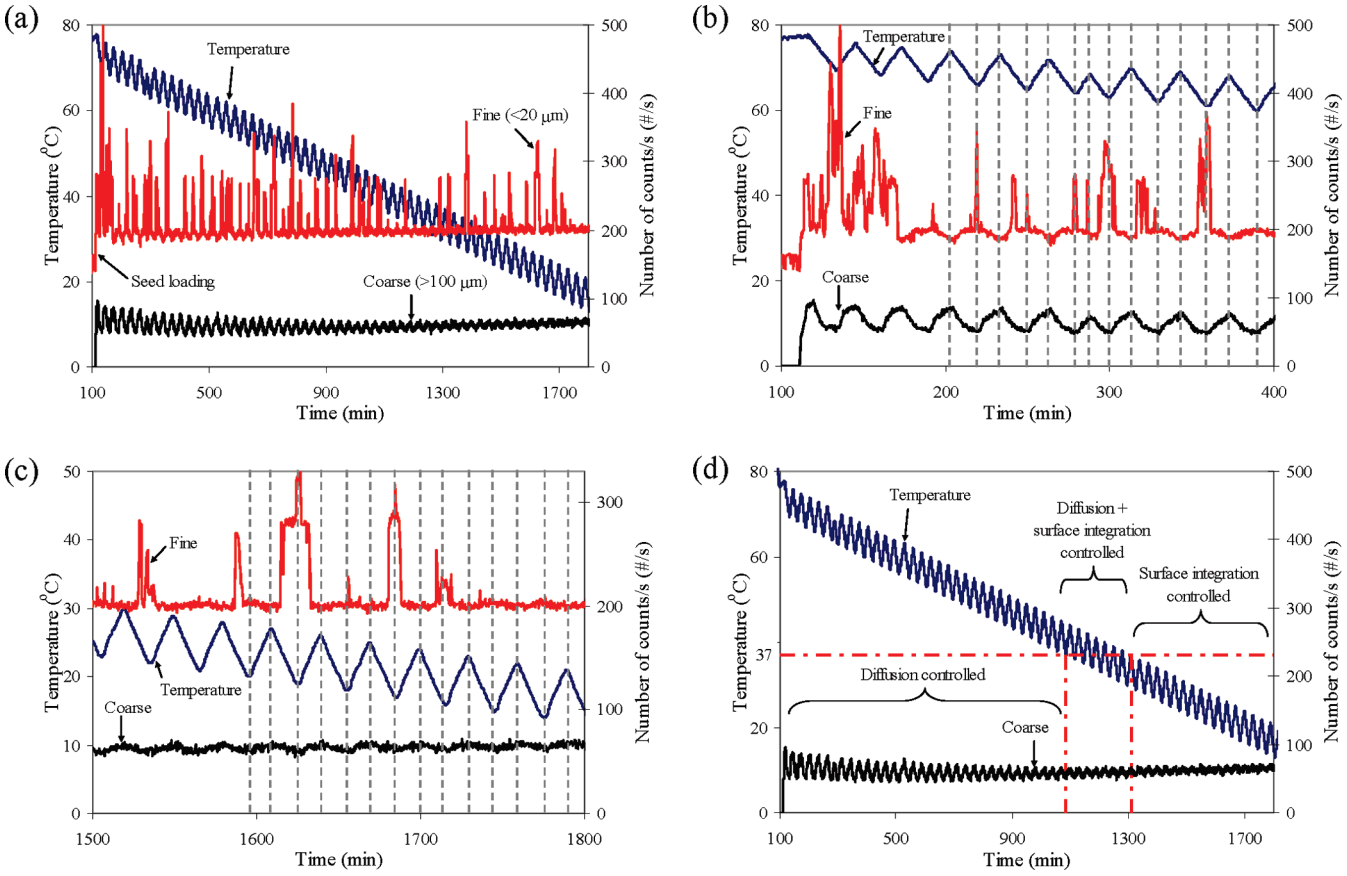

Figure 3. Profiles of temperature and FBRM fine and coarse counts/s of (a) the overall crystallization run; (b) a zoom-out view of the initial part (from 100 to 400 min); (c) a zoom-out view of the final part (from 1500 to 1800 min); and (d) the overall crystallization run with possible dissolution mechanisms.

Optical microscopy—the crystals were visually examined using a Leica DMLM optical microscope, and their images were captured and processed using Leica QWin software (version 3.0, Leica Microsystems Digital Imaging).

SEM—samples were sparsely sprinkled onto carbon tape attached to metal stubs before being thinly gold coated. The samples were then imaged using SEM (Cambridge Streoscan 360) fitted with an Inca X-Sight (Oxford Instruments) detector. An accelerating voltage of 10 kV was used during imaging.

AFM—a small quantity of the sample was spread and immobilized onto a double-sided adhesive tape that had been mounted onto metal stubs. Images were taken using a Veeco Explorer operated in contact mode with a silicon nitrite tip of <10 nm radius. A cantilever (Veeco 1950-00 silicon) with a nominal force constant of 0.21 N/m was utilized during imaging.

3. Results and Discussion

3.1. Seeded Batch Cooling Crystallization with Temperature Cycling for Sulfathiazole in Water. Figure 3a depicts the evolutions of temperature, FBRM fine counts, and FBRM coarse counts during the crystallization run. In this work, fine is defined as crystals with chord lengths of <20 μm, whereas coarse is defined as crystals with chord lengths of >100 μm. The total duration of the experiment was 30 h, during which, as can be seen from the figure, the number of fines fluctuated with the change in temperature, due to repeated nucleation and dissolution events. The number of coarse crystals fluctuated in a similar way and, as can be seen more clearly from a zoomed out view of the initial part of the profiles (from 100 to 400 min) in Figure 3b, the number of fine and coarse crystals responded to temperature change out-of-phase with each other (dashed lines were drawn to facilitate the observation): on heating, the number of fine crystals dropped while the number of coarse crystlas increased, whereas on cooling, the fine crystals increased while the coarse crystals were reduced. According to Jordan and Carless,[29] crystal growth of sulfathiazole under temperature cycling occurs by a dissolution−crystallization−dissolution−recrystallization process. It is expected that the dissolutions take place during heating phases, whereas the crystallization and recrystallization processes are promoted by cooling phases. Although the response of the number of fine crystals to the temperature change is in line with the expectation, the response of the number of coarse crystals is the opposite. A zoomed out view of the last part of the profiles (from 1500 to 1800 min) in Figure 3c shows that although the amplitude of the fluctuations of both fine and coarse crystal counts/s has significantly reduced, they are still out-of-phase with each other in response to the temperature change. Carless and Jordan[30] postulated that, under temperature cycling, the dissolution rate constants of sulfathiazole crystals are controlled by the surface integration occurring at the solid−liquid boundary at temperatures below 37 °C. Above 37 °C, the surface integration became very rapid so that the dissolution was only controlled by the diffusion of the dissolved solid away from the solid surface.[30] Figure 3d shows that the overall trend of the number of coarse crystals in response to the temperature change satisfies the division in accordance with the postulated dissolution mechanisms: (i) diffusion controlled; (ii) diffusion + surface integration controlled; and (iii) surface integration controlled.

3.2. Optical Microscopy, SEM, and AFM Images of Crystals. Figure 4 shows the position of sampling points on the

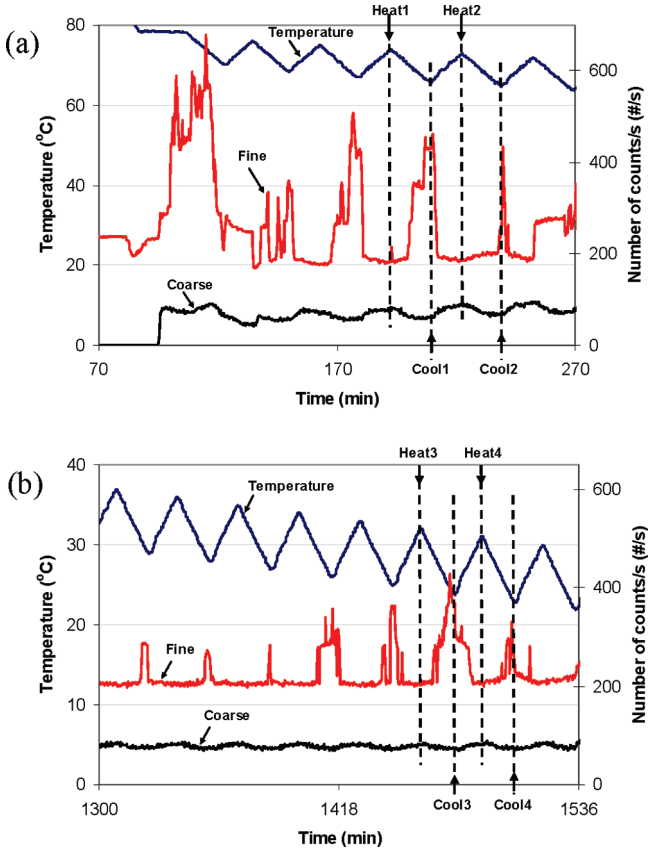

Figure 4. Sampling points on the profiles of temperature and FBRM fine and coarse counts/s at (a) the initial phase of the batch and (b) the final phase of the batch.

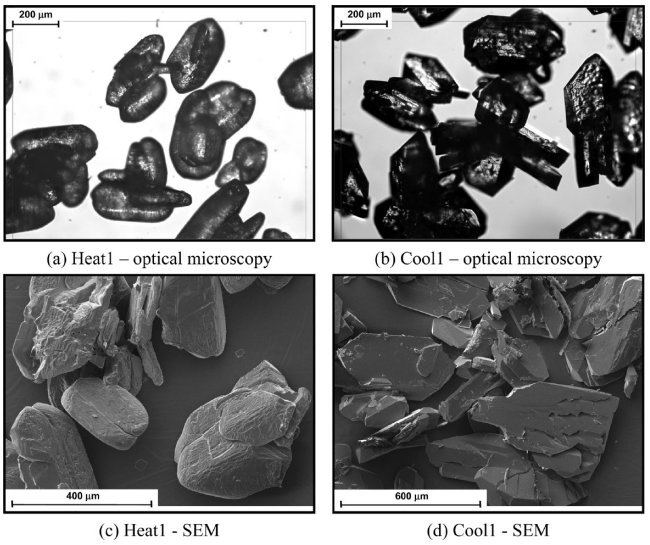

Figure 5. Optical microscopy images of (a) Heat1 and (b) Cool1; and SEM images of (c) Heat1 and (d) Cool1 crystals.

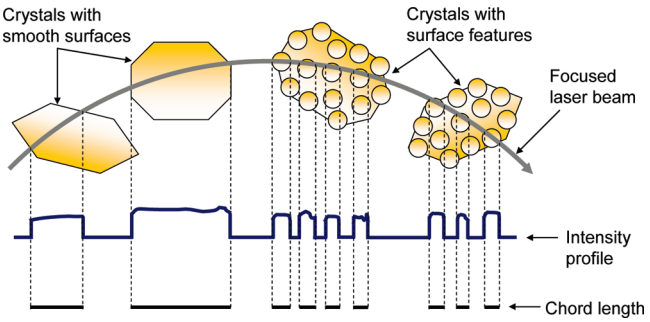

Figure 6. Schematic diagram of backscattered light pulses detection and chord length measurement of typical crystals with smooth surfaces and with surface features.

profiles of temperature and FBRM fine and coarse counts/s at the initial phase (Figure 4a) and at the final phase (Figure 4b) of the repeated crystallization process. The process was conducted with identical conditions to those of the experiment shown in Figure 3. Some samples were withdrawn during the process. Samples taken at the ends of the heating phases are denoted as "Heat1", "Heat2", "Heat3", and "Heat4", whereas samples taken at the subsequent ends of the cooling phases are denoted as "Cool1", "Cool2", "Cool3", and "Cool4".

Figure 5 shows optical microscopy and SEM images of Heat1 and Cool1 crystals. It can be observed from Figure 5a and b that Heat1 crystals have smoother surfaces and blunt edges, whereas Cool1 crystals have rougher surfaces and sharper edges. The SEM images shown in Figure 5c and d agree well with the optical microscopy images except that some of the Cool1 crystals appear to have steps with edges, while others have large flat areas on their surfaces. These results indicate that, during the heating phase, some of the growths on the surface of the crystals are dissolved. As can be inferred from the optical microscopy and SEM images of Heat1 crystals, this dissolution process has effectively polished the surface and edges of the crystals. The growths however reappeared during the cooling phase. The removal and reappearance of surface features may affect the measurement of FBRM in such a way that when the FBRM sees a crystal with a smooth surface, it will measure the crystal as a coarse chord, which is representative of the overall dimension of the crystal. If the FBRM sees a crystal with a rough surface and sharp edges, it will measure a few fine chords, representative of the surface features and edges. The effects of the surface properties and the sharper edges on the FBRM measurement have respectively been noted by Ruf, Heath, and their co-workers.[31,32] The phenomenon where coarse particles with rough surface features are not recognized as one chord but as multiple fine chords is known as signal splitting[31] or chord splitting.[33] This process can be hypothetically and schematically described in Figure 6. The figure illustrates that, in the presence of features on the surface of the crystals, the FBRM light scattering intensity on the surface was distracted or distorted. On the smooth surface of the crystals, the probability for the FBRM light scattering intensity not to be distorted is greater; hence, the FBRM is most likely to measure the crystal as one coarse chord.

Another phenomenon related to surface properties that may affect the measurement of FBRM is when the laser beam strikes the surface of the crystals in a direction perpendicular to that shown in Figure 6. The phenomenon, which is schematically illustrated in Figure 7, is known as beam spreading.[32] When the FBRM laser beam strikes the crystal's smooth surface, there is a high probability of the scattered lights re-entering the FBRM's optical system with sufficiently high intensity to be differentiated from the threshold that determines the baseline for the signal, and therefore be measured. This is illustrated in Figure 7a. However, if the crystal's surface is rough, the spreading of

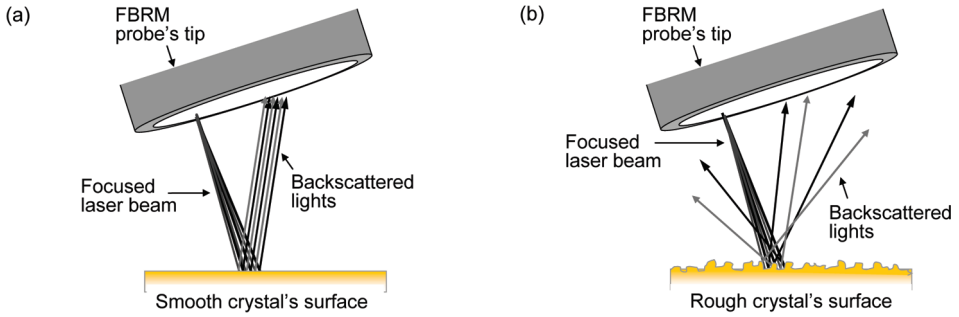

Figure 7. Schematic representations of the backscattering of the FBRM laser beam from (a) smooth and (b) rough crystal surfaces.

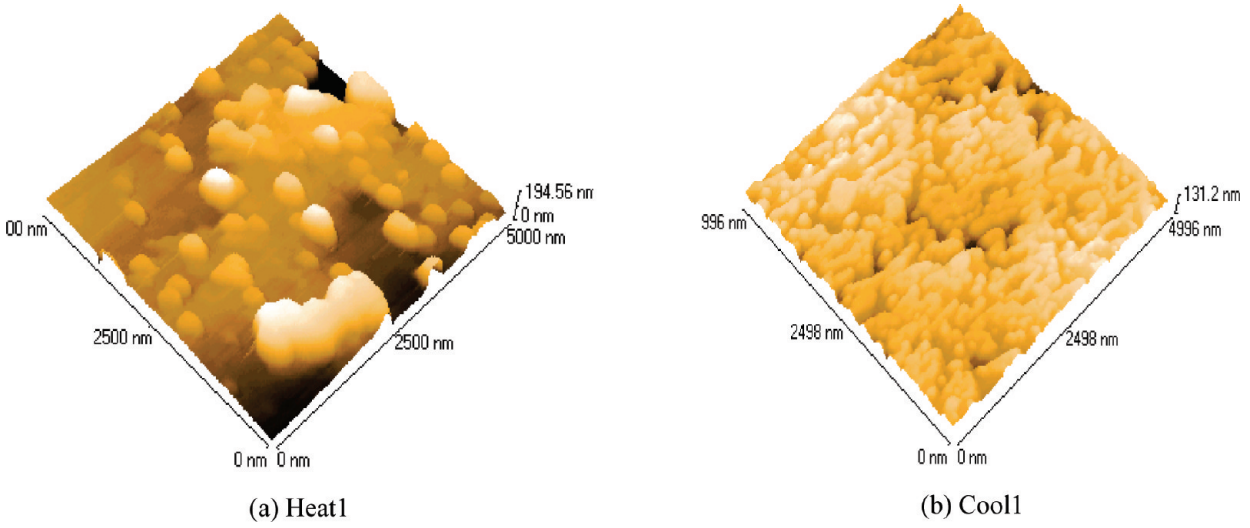

Figure 8. Five micrometer AFM images of (a) Heat1 and (b) Cool1 crystals.

the beam away from the FBRM's optical system, as shown in Figure 7b, is very likely. The small fraction of the light scattered back into the optical system produces weak light scattering intensities that the FBRM may consider only as noises. As a result, they are statistically more likely to disappear from the measured data, hence the reduction in coarse counts/s during cooling.

The AFM images of Heat1 and Cool1 crystals with a sample area size of 5 μm × 5 μm are shown in Figure 8. It can be seen that the surface of Heat1 crystals consists of nodules of variable sizes with deep valleys. The surface structure of Cool1 crystals, on the other hand, is dominated by tightly packed nodules. These AFM images are consistent with the removal and reappearance of surface features that has been deduced based on the optical microscopy and SEM images. It can be inferred from the images in Figure 8 that, on heating, the dissolution has proceeded by a pitting and layer-stripping process,[34] which in the end left some sturdy nodules and created valleys on the surface. This prepares the crystal surface with vacancies and kinks. During cooling, the supersaturation increases and the growth is facilitated on the surface features. Based on the image in Figure 8b, the growth of the crystal surface on cooling appears to follow the continuous growth model. The model, also known as the Kossel's model,[34] envisages that loosely adsorbed growth units incorporated into the crystal surface at kinks and the build-up continued until the surface is eventually covered. The loosely adsorbed growth units would be stripped away from the surface during dissolution; hence, the crystal

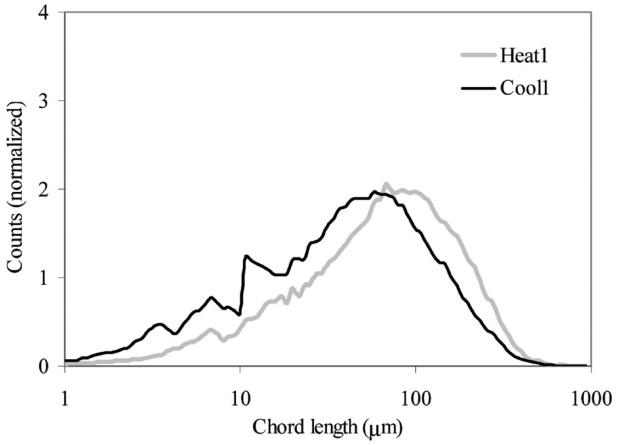

Figure 9. Comparison of the unweighted CLDs at Heat1 and Cool1.

surface with the same features as the image in Figure 8a is expected to reappear at the end of the subsequent heating phase. This observation is also in agreement with the surface-roughening theory,[35] which suggests that, under equilibrium or near-equilibrium growth conditions, surface roughening can take place by the vanishing and rounding of a planar facet. In this case, when the temperature is increased, the supersaturation decreases, bringing the system close to equilibrium, which facilitates the roughening mechanism, which drives the surface toward a shape with cusplike surface valleys. The surface roughening phenomenon in organic crystals has been discussed by Bennema,[36] and its application

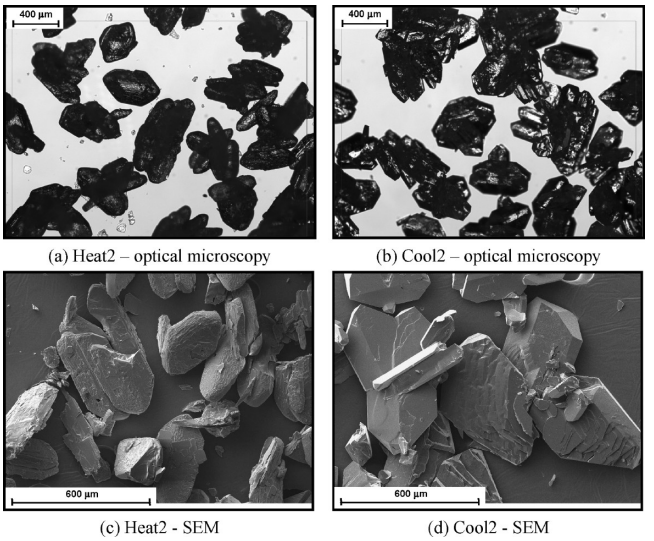

Figure 10. Optical microscopy images of (a) Heat2 and (b) Cool2, and SEM images of (c) Heat2 and (d) Cool2 crystals.

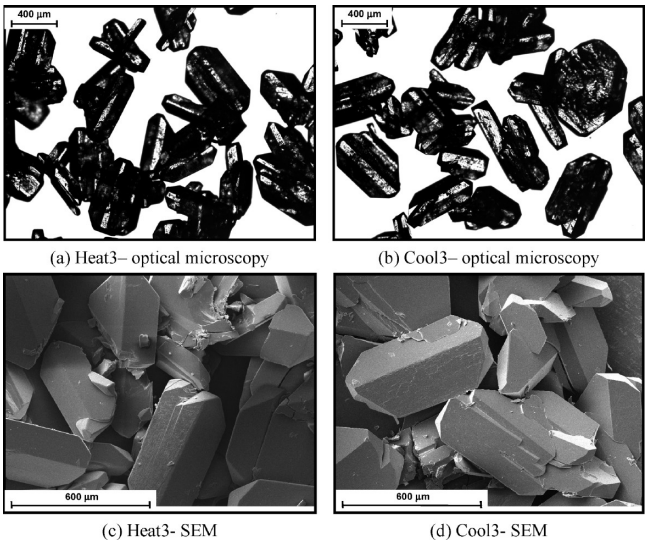

Figure 11. Optical microscopy images of (a) Heat3and (b) Cool3, and SEM images of (c) Heat3 and (d) Cool3 crystals.

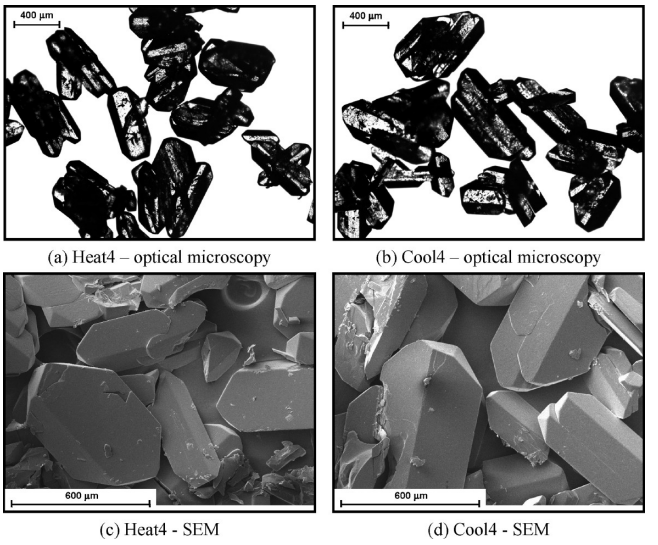

Figure 12. Optical microscopy images of (a) Heat4 and (b) Cool4, and SEM images of (c) Heat4 and (d) Cool4 crystals.

in microelectronics has been intensively studied.[37] In a recent study of fat phase crystallization in milk chocolate, Sonwai and Rousseau[38] have observed the same phenomenon, which was also promoted by temperature cycling.

The AFM images in Figure 8 also reveal that the heights of the crystals' surface features are at the nanometer scale. This information eliminates the signal/chord splitting due to the surface features as one of the possible causes for the FBRM results, since the smallest size of the chord the FBRM can measure is around 0.5 μm. However, the possible effect of the sharp edges on the FBRM measurement still remains because the SEM image in Figure 5d indicates that the edges are large enough to be measured by the FBRM.

Figure 9 compares the chord length distributions (CLDs), which are normalized to 100, at Heat1 and Cool1. It can be observed that the CLD of Heat1 is relatively narrower with a larger contribution of the coarser chords. Besides having a broader CLD and a larger contribution of the smaller chords, the CLD of Cool1 also has a higher shoulder at the small chord lengths. The trend of these CLDs is consistent with those reported by Pons and co-workers[39] in their evaluation study on the effect of faceting on the CLD. They have found that as the number of facets on a polyhedron increases, the CLD shifts more to the right, and the shoulder on the CLD reduces. This is due to the fact that the increase in the number of facets turns the overall shape of the polyhedron toward a sphere.

Figure 10 shows optical microscopy and SEM images of Heat2 and Cool2 crystals. As can be observed from the images, Heat2 and Cool2 crystals exhibit similar properties to Heat1 and Cool1 crystals, respectively. This, however, should be expected, since they are only a temperature cycle away from each other (approximately 30 min). The results show the repeatability and consistency of the occurrence of the removal and reappearance of surface features.

Optical microscopy and SEM images of Heat3 and Cool3 crystals are presented in Figure 11. The crystals were sampled approximately 22 h after the seed loading and approximately 20 h after the sampling of Heat2 and Cool2 crystals. For crystals that are suspended in a saturated solution while undergoing temperature cycling for 20 to 22 h, it is expected that they will grow in size. Some increase in the average dimension of the crystals can be observed from the optical microscopy images in Figure 11a and b in comparison to those in Figure 10a and b. In contrast to those of Heat1, Cool1, Heat2, and Cool2 crystals, the optical microscopy and SEM images of Heat3 and Cool3 crystals in Figure 11 are much more similar in their surface appearance. The heating phase did not seem to result in the smoothing or polishing of the surfaces and edges of the crystals, and the cooling phase did not appear to cause any growing of surface features. This could be due to the fact that as the process is moving toward lower temperature, the supersaturation keeps reducing until it cannot be consumed in growing surface features anymore. In addition, since the crystals were suspended in the solution for quite a long time, the crystals became aged and hard. As a result, the temperature cycling gave no effect to their surface structure. This may explain the reason why, toward the end of the crystallization batch, the amplitude of the fluctuations of both fine and coarse counts/s in response to the temperature change has reduced significantly, as shown in Figure 3c.

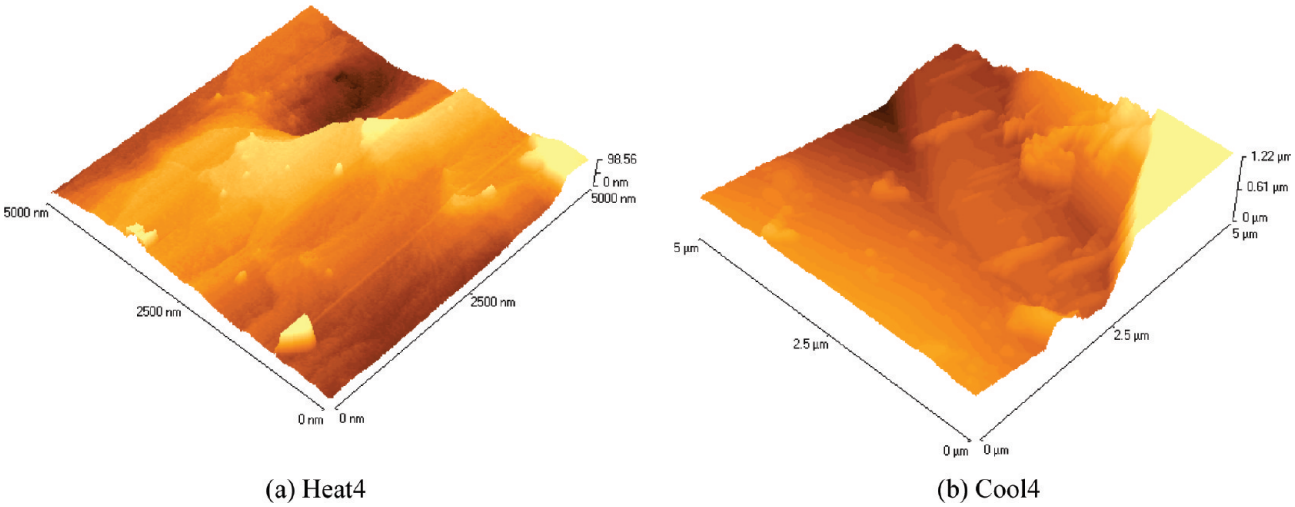

Figure 13. Five micrometer AFM images of (a) Heat4 and (b) Cool4 crystals.

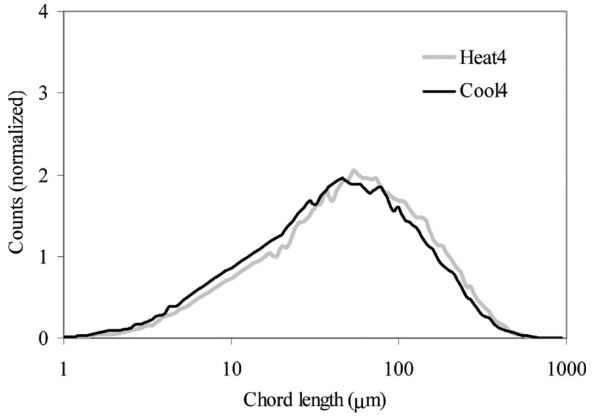

Figure 14. Comparison of the unweighted CLDs at Heat4 and Cool4.

Figure 12 shows optical microscopy and SEM images of Heat4 and Cool4 crystals. Similarly to those of Heat3 and Cool3 crystals, no significant difference in surface appearance can be observed between Heat4 and Cool4 crystals. Based on their SEM images, most crystals have flat surfaces and sharp edges. The AFM images of Heat4 and Cool4 crystals are shown in Figure 13. Although the surface of Heat4 crystals seems to be slightly affected by the dissolution process; based on the presence of surface vacancies and kinks that can be observed with a careful examination, the effect however is not as prominent as the one shown by Heat1 crystal in Figure 8a. As mentioned previously, this is probably due to the fact that the maximum temperature during heating phases toward the end of the crystallization run was not high enough to make a great impact on the surface of the already hard crystals. No extensive growths are found on the surface of Cool4 crystal, as can be seen in Figure 13b. A possible explanation for this is that the surface nucleation is unlikely to occur at low supersaturation. The change in the crystal surface properties during the temperature cycling may be observed *in situ* using endoscopy techniques, such as optical microscopy, noninvasive video-imaging systems, and Lasentec's in-process video microscopy.[40−43] It was found that good magnification can be achieved if the focus point is moved from the liquid bulk to close to the endoscope lens.[43]

Figure 14 compares the CLDs (normalized to 100) at Heat4 and Cool4. It can be seen that although the CLD at point Heat4 is slightly shifted to the right, the difference between them is not as large as the difference between the CLDs at Heat1 and Cool1, shown previously in Figure 9. The trend of these CLDs agrees well with the inference made based on the microscopy analyses that Heat4 and Cool4 crystals are very similar in their surface appearance.

Two possible explanations for the out-of-phase profiles of the FBRM's fine and coarse counts/s in response to the temperature change put forward earlier, i.e. the signal/chord splitting and the beam spreading, are related to the surface features. There is a possible explanation for the FBRM's result that is independent of the surface features. This explanation is related to the depth of penetration of the FBRM laser beam as a function of crystal size and number density of crystals. For example, in a suspension of low concentration of coarse crystals, the laser beam can penetrate far into the medium being measured, which then causes the signal threshold to reduce. This provides a high effective swept volume and allows crystals far away from the focal point, i.e. weaker reflectors, to be measured. The effect of the distance between crystals and the focal point to the FBRM signal is described schematically in Figure 15. If now a high concentration of fine crystals is added to the suspension, the following may occur: (a) Due to the volume exclusion effect, the fine crystals tend to be suspended between the probe window and the coarse crystals—this effectively masks the coarse crystals from being in contact with the laser beam. As a result, the FBRM will measure the fine particles rather than the coarse particles. (b) The increase in the solid density will increase the background backscatter level. This in turn causes the signal threshold to increase, which means that it is more difficult to see weak reflective particles. Since particles that are larger or farther away will be weaker reflectors, it is statistically more likely these will disappear from the measured data. (c) The increased number of fine crystals will scatter, reflect, or absorb the laser light more, which means that the effective penetration depth of the laser is shortened. This consequently will reduce the effective swept volume of the laser, reducing the count rate, especially of the coarse crystals. It is expected that, during heating, some of the fine crystals will dissolve and this will expose the coarse crystals to the laser beam. As a result, the fine counts/s reduces and

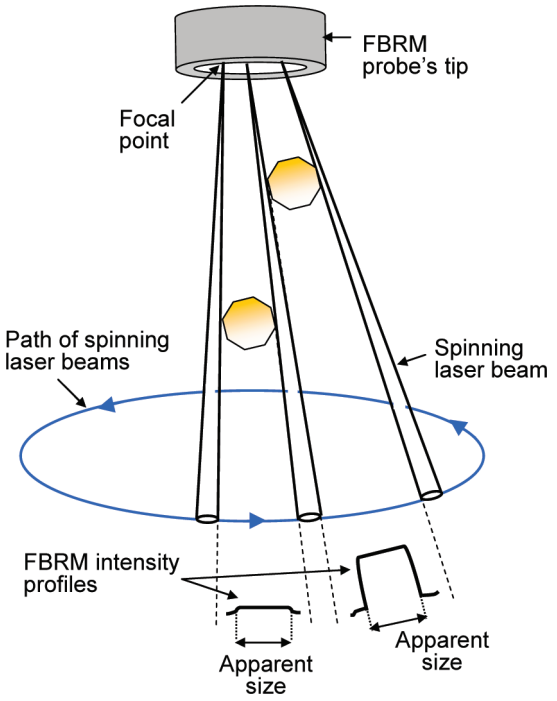

Figure 15. Effect of the distance between crystals and the focal point on the FBRM signal (modified from Pons and co-workers[39]).

the coarse counts/s increases. During cooling, the fine crystals will renucleate and subsequently will return to obstruct the coarse crystals from the laser beam; this will result in an increase in the fine counts/s and a reduction in the coarse counts/s. The phenomenon described above is briefly mentioned by Ruf and co-workers,[31] in which it was referred to as a "masking effect". It is also called a "snowstorm effect"[44] because of its similarity to the visual limitation during a snowstorm when larger objects further away, which are perfectly visible in clear weather, became difficult to observe or completely invisible due to a dense layer of small snow particles. In the case of very high population of fine particles, they will be very close to each other; hence, the difference between the intensity profiles of the backscattered light from the particles in the focal point of the laser beam, or slightly further, will not be significant. This is because in such a case there is a high probability that the laser beam, after passing across one particle, will immediately meet another small particle, which will reflect with similar intensity, making the differentiation of individual chord lengths difficult. In extreme cases, the continuous reflection with small variations in intensity can be considered by the instrument as noise in an increased signal threshold level and the particles may "disappear" completely from the FBRM measurement. This is similar to the case when very heavy snowfall may appear as a continuous white curtain with indistinguishable snow particles, obscuring larger objects farther away. A schematic representation of the snowstorm effect is presented in Figure 16.

The snowstorm effect, however, is not the likely cause for the behavior of the FBRM data produced in this work because of the following reasons: (a) the effect only occurs when a system has a very high population of very fine crystals compared to the coarse crystals. The count rate of those fine crystals should be on the order of several thousand counts/s.[44] In this work, the overall count rate of the fine crystals was very low; which was around 200−300 count/s (see Figure 3a). The number is,

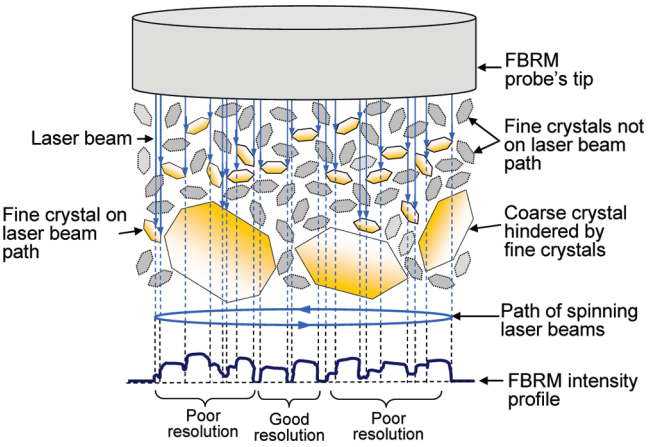

Figure 16. Schematic representation of the "snowstorm effect".

therefore, insufficient for the snowstorm effect to take place; (b) the fine crystals need to be very small compared to the size of the coarse crystals; their size should be 2 orders of magnitude smaller than that of the coarse crystals.[44] Based on the microscopic images of the crystals (see Figures 5, 10, 11, and 12), the identified fine crystals in this work are only a little smaller than the coarse particles. In order for the snowstorm effect to occur, a much greater difference in size is required; and (c) as can be observed from the profiles of the FBRM fine and coarse counts/s shown in Figure 3a, the number of fine crystals is consistent throughout the experiment; they fluctuated during heating and cooling within the same range. However, the amplitude of the fluctuations in the number of coarse crystals significantly reduced during the experiment. If these fluctuations were caused by the snowstorm effect, they should have been relatively consistent during the entire duration of the experiment, similarly for the consistent fluctuations in the number of fines. The analysis of the potential causes of the observed fluctuations in the FBRM fine and coarse counts indicates that the most likely explanation is based on a combination effect of signal spreading, which correlates with changes in surface roughness, and signal/chord splitting, which is in correlation with the formation of sharp edges.

4. Conclusions

The effect of temperature cycling on the surface features of sulfathiazole crystals was investigated using *in situ* FBRM and *ex situ* optical microscopy, SEM, and AFM. It was observed that, during the initial stage of the crystallization process, during which the average process temperature was higher, the heating phases resulted in crystals with smooth surfaces, while the cooling phases resulted in crystals with features grown on their surfaces. During the final stage of the crystallization process, during which the average process temperature was lower, the effect of both heating phases and cooling phases on the surface appearance of the crystals was not that significant. This is probably because the supersaturation was already depleted and the crystals turned harder. It was also found that the insight into these surface events was detected by FBRM as a result of a combination of beam-spreading caused by changes even at the nanometer scale and signal/chord splitting due to the formation of sharp edges. The study indicates that FBRM may provide useful information related to the potential changes in the surface properties of the crystalline products, which can be used to avoid problems in

the downstream processing or in the final product property due to variations in flowability and friability.

Acknowledgment. Ian Haley from Mettler Toledo, U.K., is acknowledged for providing valuable technical advice on FBRM. The authors thank Frank Page for the SEM imaging and David Grandy for the AFM analysis—all were carried out in the Department of Materials, Loughborough University. Financial support provided by the Engineering and Physical Sciences Research Council (EPSRC), U.K. (Grant EP/E022294/1), is also gratefully acknowledged. The first author is grateful to the Malaysian Ministry of Higher Education for a scholarship.

References

(1) Woo, X. Y.; Nagy, Z. K.; Tan, R. B. H.; Braatz, R. D. *Cryst. Growth Des.* **2009**, *9* (1), 182.
(2) Abu Bakar, M. R.; Nagy, Z. K.; Rielly, C. D. *Org. Process Res. Dev.* **2009**, *13*, 1343–1356.
(3) Loi Mi Lung-Somarriba, B.; Moscosa-Santillan, M.; Porte, C.; Delacroix, A. *J. Cryst. Growth* **2004**, *270*, 624.
(4) Moscosa-Santillan, M.; Bals, O.; Fauduet, H.; Porte, C.; Delacroix, A. *Chem. Eng. Sci.* **2000**, *55*, 3759–3770.
(5) Barrett, P.; Smith, B.; Worlitschek, J.; Bracken, V.; O'Sullivan, B.; O'Grady, D. *Org. Process Res. Dev.* **2005**, *9*, 348–355.
(6) Carless, J. E.; Foster, A. A. *J. Pharm. Pharmacol.* **1966**, *18*, 697–708.
(7) Chew, J. W.; Black, S. N.; Chow, P. S.; Tan, R. B. H. *Ind. Eng. Chem. Res.* **2007**, *46*, 830–838.
(8) Zhou, G. X.; Fujiwara, M.; Woo, X. Y.; Rusli, E.; Tung, H.; Starbuck, C.; Davidson, O.; Ge, Z.; Braatz, R. D. *Cryst. Growth Des.* **2006**, *6*, 892–898.
(9) Liotta, V.; Sabesan, V. *Org. Process Res. Dev.* **2004**, *8*, 488–494.
(10) Barrett, P.; Glennon, B. *Chem. Eng. Res. Des.* **2002**, *80*, 799–805.
(11) Simon, L. L.; Nagy, Z. K.; Hungerbuehler, K. *Chem. Eng. Sci.* **2009**, *64*, 3344–3351.
(12) Simon, L. L.; Oucherif, K. A.; Nagy, Z. K.; Hungerbuhler, K. *Chem. Eng. Sci.*, **2010**, *65*, 4983−4995.
(13) Fujiwara, M.; Chow, P. S.; Ma, D. L.; Braatz, R. D. *Cryst. Growth Des.* **2002**, *2*, 363–370.
(14) Abu Bakar, M. R.; Nagy, Z. K.; Rielly, C. D. *Cryst. Growth Des.* **2009**, *9* (3), 1378–1384.
(15) Chew, J. W.; Chow, P. S.; Tan, R. B. H. *Cryst. Growth Des.* **2007**, *7*, 1416–1422.
(16) Barthe, S.; Rousseau, R. W. *Chem. Eng. Technol.* **2006**, *29*, 206–211.
(17) Yu, Z. Q.; Chow, P. S.; Tan, R. B. H. *Ind. Eng. Chem. Res.* **2006**, *45*, 438–444.
(18) Yi, Y. J.; Myerson, A. S. *Chem. Eng. Res. Des.* **2006**, *84*, 721–728.
(19) Nagy, Z. K. *Comput. Chem. Eng.* **2009**, *33*, 1685–1691.
(20) O'Sullivan, B.; Barrett, P.; Hsiao, G.; Carr, A.; Glennon, B. *Org. Process Res. Dev.* **2003**, *7*, 977–982.
(21) O'Sullivan, B.; Glennon, B. *Org. Process Res. Dev.* **2005**, *9*, 884–889.
(22) Shaikh, A. A.; Salman, A. D.; Mcnamara, S.; Littlewood, G.; Ramsay, F.; Hounslow, M. J. *Ind. Eng. Chem. Res.* **2005**, *44*, 9921–9930.
(23) Scholl, J.; Bonalumi, D.; Vicum, L.; Mazzotti, M.; Muller, M. *Cryst. Growth Des.* **2006**, *6*, 881–891.
(24) Doki, N.; Seki, H.; Takano, K.; Asatani, H.; Yokota, M.; Kubota, N. *Cryst. Growth Des.* **2006**, *4*, 949–953.
(25) Hukkanen, E. J.; Braatz, R. D. *Sens. Actuators, B* **2003**, *96*, 451–459.
(26) Castle, J. E.; Zhdan, P. A. *J. Phys. D: Appl. Phys.* **1997**, *30*, 722–740.
(27) Hansma, P. K.; Elings, V. B.; Marti, O.; Bracker, C. E. *Science* **1989**, *242*, 209–216.
(28) Drake, B.; Prater, C.; Weisenhorn, A.; Gould, S.; Albrecht, T.; Quate, C.; Cannell, D.; Hansma, H.; Hansma, P. *Science* **1989**, *243*, 1586–1589.
(29) Jordan, D.; Carless, J. E. *J. Pharm. Pharmacol.* **1976**, *28*, 410–414.
(30) Carless, J. E.; Jordan, D. *J. Pharm. Pharmacol.* **1974**, *26* (Suppl.), 86P–87P.
(31) Ruf, A.; Worlitschek, J.; Mazzotti, M. *Part. Part. Syst. Charact.* **2000**, *17*, 167–179.
(32) Heath, A. R.; Fawell, P. D.; Bahri, P. A.; Swift, J. D. *Part. Part. Syst. Charact.* **2002**, *19*, 84–95.
(33) Kail, N; Briesen, H.; Marquardt, W. *Powder Technol.* **2008**, *185*, 211–222.
(34) Mullin, J. W. *Crystallization*; Butterworth-Heinemann: London, 2001.
(35) Burton, W. K.; Cabrera, N.; Frank, F. C. *Philos. Trans. R. Soc. A* **1951**, *243*, 299–360.
(36) Bennema, P. *J. Cryst. Growth* **1994**, *122*, 110–119.
(37) Alivisatos, A. P. *MRS Bull.* **1998**, *23* (2), 18–23.
(38) Sonwai, S.; Rousseau, D. *Food Chem.* **2010**, *119*, 286–297.
(39) Pons, M.-N.; Milferstedt, K.; Morgenroth, E. *Chem. Eng. Sci.* **2006**, *61*, 3962–3973.
(40) Patience, D. B.; Dell'Orco, P. C.; Rawlings, J. B. *Org. Process Res. Dev.* **2004**, *8*, 609–615.
(41) Calderon De Anda, J.; Wang, X. Z.; Roberts, K. J. *Chem. Eng. Sci.* **2005**, *60*, 1053–1065.
(42) Wang, X. Z.; Roberts, K. J.; Ma, C. *Chem. Eng. Sci.* **2008**, *63*, 1173–1184.
(43) Simon, L. L.; Nagy, Z. K.; Hungerbuehler, K. *Org. Process Res. Dev.* **2009**, *13*, 1254–1261.
(44) Haley, I. Personal communication, March 30, 2010, Technology & Application Consultant, Mettler-Toledo Ltd, U.K.